AD-A045 017 BRANDEIS UNIV WALTHAM MASS DEPT OF PHYSICS F/G 3/2
SOLAR ATMOSPHERIC DYNAMICS.(U)
MAY 77 R F STEIN F19628-75-C-0013

UNCLASSIFIED AFGL-TR-77-0108 NL

1 OF 1
AD
A045017

END
DATE
FILMED
10-77
DDC

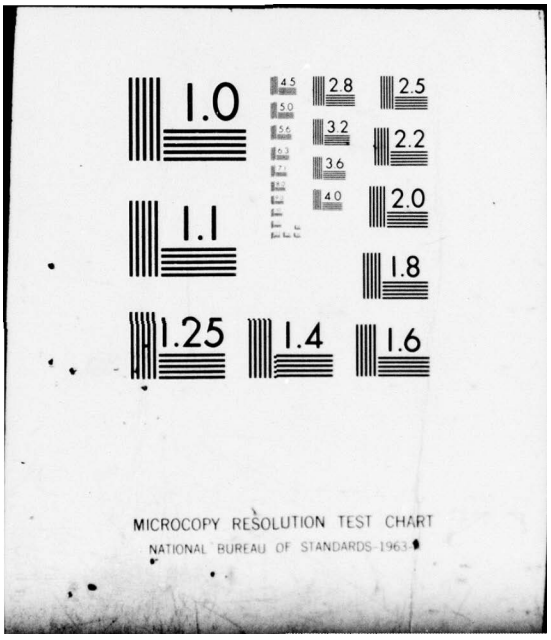
1.0
1.1
1.25
1.4
1.6
1.8
2.0
2.2
2.5
2.8
3.2
3.6
4.0
4.5
5.0
5.6
6.3
7.1
MICROCOPY RESOLUTION TEST CHART
NATIONAL BUREAU OF STANDARDS-1963-A

AFGL-TR-77-0108

12

SOLAR ATMOSPHERIC DYNAMICS

R.F. Stein, Principal Investigator

Physics Department
Brandeis University
Waltham, MA. 02154

May 1977

Final Report

19 September 1974 - 30 September 1976

Approved for public release;
distribution unlimited

Air Force Geophysics Laboratory
Air Force Systems Command
United States Air Force
Hamscom AFB, Massachusetts 01731

SECURITY CLASSIFICATION OF THIS PAGE (When Data Entered)

REPORT DOCUMENTATION PAGE

READ INSTRUCTIONS BEFORE COMPLETING FORM

1. REPORT NUMBER: AFGL-TR-77-0108	2. GOVT ACCESSION NO.
3. RECIPIENT'S CATALOG NUMBER	
4. TITLE (and Subtitle): SOLAR ATMOSPHERIC DYNAMICS.	5. TYPE OF REPORT & PERIOD COVERED: Final Report. 19 Sep 74 - 30 Sep 76.
	6. PERFORMING ORG. REPORT NUMBER
7. AUTHOR(s): R.F. Stein	8. CONTRACT OR GRANT NUMBER(s): F19628-75-C-0013
9. PERFORMING ORGANIZATION NAME AND ADDRESS: Physics Department, Brandeis University, Waltham, MA. 02154	10. PROGRAM ELEMENT, PROJECT, TASK AREA & WORK UNIT NUMBERS: 62101F, 76490615
11. CONTROLLING OFFICE NAME AND ADDRESS: Air Force Geophysics Laboratory, Hanscom AFB, Massachusetts 01731, Monitor/Richard Altrock/PH	12. REPORT DATE: May 1977
	13. NUMBER OF PAGES: 20
14. MONITORING AGENCY NAME & ADDRESS (if different from Controlling Office)	15. SECURITY CLASS. (of this report): UNCLASSIFIED
	15a. DECLASSIFICATION/DOWNGRADING SCHEDULE

16. DISTRIBUTION STATEMENT (of this Report)

Approved for public release; distribution unlimited

17. DISTRIBUTION STATEMENT (of the abstract entered in Block 20, if different from Report)

18. SUPPLEMENTARY NOTES

400 536

19. KEY WORDS (Continue on reverse side if necessary and identify by block number)

Solar Chromospheric heating
Solar Coronal heating
Magneto-acoustic gravity waves

20. ABSTRACT (Continue on reverse side if necessary and identify by block number)

This study seeks to calculate the generation and propagation of Magneto-Acoustic Gravity (M.A.G.) waves in the solar atmosphere and their effect on the heating of the chromosphere and corona. A computer program has been written, which is capable of integrating the equations of motion of such waves, which are inherently three-dimensional. To simplify the equations, without seriously distorting the nature of the motions, we impose a fixed horizontal modal structure consisting of 6 waves propagating horizontally in a hexagonal pattern. These equations need to be integrated in time and only one spatial direction - the vertical.

DD FORM 1 JAN 73 1473 EDITION OF 1 NOV 65 IS OBSOLETE

The program is currently being tested for the simpler case of non-vertically propagating acoustic-gravity waves.

We have also analyzed Skylab UV data for evidence of acoustic pulses in the transition region and calculated the steady state structure of the solar wind flow along a magnetic flux tube that diverges more rapidly than vertically.

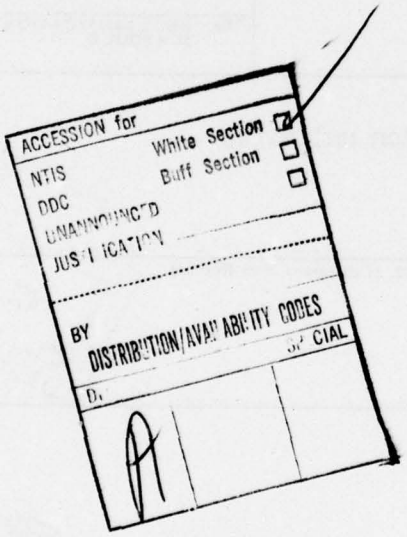

SOLAR ATMOSPHERIC DYNAMICS

I. Introduction

The goal of this research is to study the driving of the solar atmospheric oscillations and their role in heating the chromosphere and corona. During the first year of this contract the wave vector surfaces of Magneto-Acoustic-Gravity (M.A.G.) waves were studied and we derived modal equations for compressible three-dimensional fluid flow that will enable the propagation and dissipation of M.A.G. waves to be studied. During the second year a computer code to solve these modal equations was written and testing on it begun. In addition, data from Skylab was analyzed for acoustic pulses in the transition region and the steady flow of a solar wind through a magnetic flux tube diverging more rapidly than radially was calculated. The contract supported Dr. S.H. Hsieh as a research fellow and Mr. Robert Wolff as a graduate student working on the solution of the modal equations. So far under this contract one paper has been published on Magneto-Gravity Waves (Schwartz and Stein, 1975), and two others are now being prepared. One on "Magneto-Acoustic-Gravity Waves" and the other on "Flow Through a Diverging Magnetic Flux Tube".

II. Wave Vector Surfaces of Magneto-Acoustic-Gravity Waves

I have studied the wave vector surfaces of Magneto-Acoustic-Gravity (MAG) waves in the WKB limit, that is using the local dispersion relation. The wave vector surface is the surface $\underset{\sim}{k}(\omega)$ in $\underset{\sim}{k}$-space on which the local dispersion relation is satisfied for fixed frequency ω.

There are three wave modes. One is the usual Alfvèn mode. It's wave vector surface consists of two planes perpendicular to the magnetic field and a distance $\omega/a\cos\theta$ from the origin. We call these the Alfvèn planes.

At high frequencies, $\omega > N_{ac}$, gravity is unimportant. Here $N_{ac}=rg/2s$ is the acoustic cutoff frequency, where g is the acceleration of gravity, s is the sound speed and r the ratio of specific heats at constant pressure and volume. In this case, the MAG waves behave as Magneto-hydrodynamic (MHD) waves. In weak magnetic fields the fast mode is an acoustic mode and the slow mode a magnetic mode, while in strong magnetic fields the fast mode is a magnetic pressure mode and the slow mode an acoustic mode propagating along the magnetic field.

At low frequencies, one mode has a wave vector surface that is approximately a plane perpendicular to the magnetic field. This wave vector surface lies everywhere closer to the origin than the Alfvèn plane and has an outward bump that just touches the Alfvèn plane for vertically propagating waves ($k_{Horiz}=0$). At large k_x, the wave vector surface approaches a plane that passes through the origin.

The other mode's wave vector surface is similar to the acoustic-gravity wave hyperboloid close to the origin and also becomes a plane, perpendicular to the magnetic field far away from the origin. As the magnetic field strength increases, the hyperboloid gets squashed between the Alfvèn planes and disappears. In the regions of large K_{Horiz} neither wave is a normal propagating wave. For both their potential energy becomes far greater than their kinetic energy. In the weak field case the magnetic potential energy is small for both modes when K_{Horiz} is large, while in the strong field case one mode has predominantly magnetic potential energy and the other has none.

Part of this work was published by Schwartz and Stein (1975) and part

appeared in a thesis of Nelson Hartunian (1975) from Brandeis University. The remainder is now being written up for publication. A clearer picture of MAG waves will however require the solution of the initial value problem either with the modal or a truly 3-dimensional code.

III. Modal Equations for Compressible Fluid Flows

Non-linear calculations are simple in one spatial dimension (Richtmyer and Morton, 1969), but complicated in two or three. However, gravity waves are inherently two-dimensional and magneto-acoustic-gravity waves are inherently three-dimensional. The modal approach reduces the three-dimensional problem to a one-dimensional problem by imposing a horizontal structure on the motion. We separate all the fluid variables into mean and fluctuating parts. The mean part is uniform on horizontal planes and the fluctuating part has a periodic hexagonal horizontal structure of some given length scale. We then have a system of Eulerian partial differential equations for the mean and fluctuating variables. These equations were derived in collaboration with H.S. Hsieh and Robert Wolff.

To solve these equations we write them in finite difference "conservation" form and use the Richtmyer two-step Lax-Wendroff method (Richtmyer and Morton, 1969):

$$u_{j+\frac{1}{2}}^{n+\frac{1}{2}} = \tfrac{1}{2}(u_j^n + u_{j+1}^n) - \frac{\Delta t}{2\Delta x}(F_{j+1}^n - F_j^n) + \frac{\Delta t}{2} S_{j+\frac{1}{2}}^n$$

$$u_j^{n+} = u_j^n - \frac{\Delta t}{\Delta x}(F_{j+\frac{1}{2}}^{n+\frac{1}{2}} - F_{j-\frac{1}{2}}^{n+\frac{1}{2}}) + \Delta t\, S_j^{n+\frac{1}{2}}$$

The Lax-Wendroff scheme is dissipative and handles shocks well, but it also damps waves with wavelengths less than 20 zones moderately. It is also subject to some non-linear instabilities. To suppress these instabilities we introduce additional dissipation with the "flux corrected transport" scheme developed by J. Boris (Book, Boris, Hain 1975). The Lax-Wendroff scheme was tested for the one-dimensional full fluid equations on the shock tube problem and a small amplitude piston driven wave in a uniform medium. The shock tube problem is an especially sensitive test because it involves three types of waves (shock, contact discontinuity and simple wave) with known speeds and amplitudes, and is independdent of boundary conditions.

The boundary conditions are more difficult for the modal equations than for Lagrangian one-dimensional equations. The Richtmyer Lagrangian scheme is a leapfrog scheme with the variables staggered in space and time. Hence the boundary conditions need only specify the velocity. The Lax-Wendroff scheme defines all variables at the same space and time. Hence we must specify all the variables at the boundary. To do this we need to know the solution at one point, but in general we do not. In our case, we can use polarization relations for small amplitude waves to specify all variables at the inflow boundary. At the outflow boundary, we can use essentially the same method as in the Lagrangian scheme. For any variable f at the boundary x_J,

$$f_J^{n+} = f_J^n + (C_{J-\frac{1}{2}}^{n+\frac{1}{2}} + u_{J-\frac{1}{2}}^{n+\frac{1}{2}})\,\Delta t$$

$$(f_{J-1}^n - f_J^n)/(x_{J-1} - x_J)$$

These boundary conditions have been coded for acoustic waves in a uniform medium and the outflow boundary conditions for a stratified atmosphere as well. It remains to code the inflow boundary conditions for acoustic-gravity waves.

A computer code for the modal equations (without magnetic field or radiation) is currently being tested in collaboration with Robert Wolff. The testing program is as follows:

A. To test non-linear coupling, consider plane-parallel (vertical) motion in a uniform medium for
   (1) shock tube
   (2) piston driven sinusoidal waves including shock formation

B. To test horizontal variation, consider a piston driven wave in a uniform medium. This corresponds to waves propagating at an angle to the vertical direction. Test:
   (1) increase in vertical wavelength with decreasing horizontal scale
   (2) velocity is longitudinal
   (3) reduced height of shock formation
   (4) boundary condition for non-vertically propagating wave

C. To test vertical motion in a stratified atmosphere, consider piston driven vertical acoustic waves with frequency above and below the critical frequency and compare with the one-dimensional Lagrangian calculations using the full fluid equations.

Once the code has been fully tested for acoustic-gravity waves, conduction and radiative losses will be added and a heating model of the solar chromosphere and corona constructed. Afterwards magnetic fields and grey radiative transfer will be added. Simultaneously, grey radiative transfer will be added to the one-dimensional Lagrangian code. The modified code will be used to construct a dynamic model solar atmosphere. This will be used as an initial model for a non-equilibrium, non-grey time dependent model, which will be used to analyze changes observed in line profile due to waves propagating through the atmosphere

in collaboration with Richard Klein (Kitt Peak National Observatory) and Richard Shine (University of Colorado). Richard Shine is currently calculating Hα emission from the accretion shock found in the calculations by Klein, Stein, and Kalkofen (1977) of a radiating shock propagating through an A star atmosphere.

The Lax-Wendroff scheme is also being used in the development of a two- and three-dimensional code in collaboration with Richard Klein and Lawrence Auer (High Altitude Observatory, National Center for Atmospheric Research). Such a code will be able to solve truly three-dimensional magneto-hydrodynamic problems. We have so far made tests on two two-dimensional problems -- a symmetric shock and gravitational accretion flow into a density perturbation. We have tested three schemes: MacCormack (1971), Lax-Wendroff and Dunner Cell (Book, Boris, and Hain, 1975). So far only the MacCormack scheme is compatible with our Poisson equation solver for the gravitational potential, but all three work for the shock problem. We are now working on the data management problem for three-dimensional calculations and on a faster Poisson solver.

IV. Wave Pulses in the Transition Region

Vertically propagating acoustic pulses develop a secondary crest in their wake (Figure 1). The second peak arises from the resonant wake behind pulses in a stratified atmosphere (Lamb, 1945; Schmidt and Zirker, 1963; Kato, 1966; Stein and Schwartz, 1972). The separation between the peaks is close to the acoustic cutoff period of the atmosphere. This two peaked wave form may be used as a signature for acoustic pulses. Observations from Skylab show intensity fluctuations in transition region lines that occasionally displayed such a double peaked structure (Figure 2) (Vernazza et al 1975). Vernazza and I have made a systematic search for such double peaked pulses, and performed some

calculations on pulse propagation to determine the relation between density and velocity fluctuations.

If acoustic pulses with their double peaked structure are present, they should become more prominant as we look at stronger pulses. Weak pulses will be common and precede other weak pulses by various time intervals without any causal connection. However, strong pulses are rare, hence two such pulses following one another closely in time are likely to be causally connected. To search for the presence of acoustic pulses in the Skylab data, we made histograms of the number of pulses seen in CIII and OIV intensity greater than a given strength versus the interval between succeeding pulses (Figures 3 and 4). When all pulses are included, the number of pulses at any given separation decreases nearly monotonically with increasing pulse separation from a maximum at the minimum resolvable separation. As the pulses included are restricted to those of greater and greater strength a decided maximum develops in the range of 100-175 seconds separation. This behavior is clearly seen in the OIV data. The data for CIII, which is formed at 9×10^4 °K, is more complicated. In the case of CIII, even for the weakest pulses, there is a maximum near 150 sec. separation, and this maximum persists as the pulse strength increases.

A separation of 150 sec. corresponds to the acoustic cutoff period in an isothermal atmosphere of 3000 °K. Note there is also a secondary maximum in both the CIII and OIV data at a separation of 250 sec., which corresponds to the acoustic cutoff period in an isothermal atmosphere of 8000 °K.

Next we looked at why waves are difficult to detect in intensity fluctuations in the transition region. We were especially interested in why the 300s oscillations stop being seen. As a simple preliminary calculation we kept the temperature of each fluid blob fixed at its initial value as the blob moved in response to waves. This case corresponds to infinitely rapid radiative energy adjustment flow. The results are shown in Figure 5. We see that when an acoustic

wave enters the transition region its velocity amplitude continues to increase with height, but its density fluctuation amplitude $\delta\rho/\rho_0$ decreases by a factor of 3. Hence the intensity fluctuation, which is proportional to density squared, will decrease by an order of magnitude.

V. Flux Tube Flow

Kopp and Holzer (1976) investigated the expansion of the solar wind along a tube that widens out faster than radially. Such a widening tube may occur in the expansion of the solar wind along open magnetic field lines. They found that when the tube, along which the fluid flows, widens by more than a critical amount the flow develops two sonic points. In the standard case of a radially diverging flow, the fluid accelerates and becomes supersonic at a sonic point located at several solar radii. When the flow diverges more rapidly than radially close to the sun, a second sonic point develops in the region of rapid divergence. Kopp and Holzer investigated the time-dependent transient behavior of the solar wind when the flux tube along which it is flowing suddenly widens by more than the critical amount. They found that the wind accelerates and becomes supersonic at the inner critical point, shocks back to the subsonic solution, then accelerates and becomes supersonic again at the outer critical point. The shock is facing inward, but is dragged outward by the expanding wind. In the course of several hours the shock is dragged out from the inner critical point to the outer critical point, Thereafter, the flow becomes supersonic at the inner critical point and remains supersonic throughout, rejoining the standard solution beyond the outer critical point.

I repeated these calculations using an initial value Lagrangian finite difference code, instead of the Eulerian code used by Kopp and Holzer. I considered the same case as they had, an isothermal atmosphere of pure hydrogen at a temperature of 1.8×10^6 °K. The area of the flux tube was widened from a

radial tube to a tube which diverged by a factor 4.5 greater than radial at half a solar radius above the surface. The formula for the diverging flux tube was the same as used by Kopp and Holzer:

$$A(r)/A_{\odot} = (r/R_{\odot})^2 \, [f_{max} \, e^{(r-R_1)/\sigma} + f_1]/[e^{(r-R_1)/\sigma} + 1]$$

where

$$f_1 = 1 - (f_{max}-1)e^{(R_{\odot}-R_1)/\sigma},$$

$$f_{max} = 4.5 \text{ and } \sigma = 0.1 \, R_{\odot}.$$

Contrary to their results, I found the shock that developed outside the inner critical point remained stationary and was not dragged outward by the wind (Figure 6).

Inside the shock the wind speed was u_0 = 231 km/s (M_0 = 1.33) and outside it was u_1 = 104 km/s (M_1 = 0.6). The sound speed was s_0 = 173 km/s. The velocity jump across the shock

$$y = \frac{u_1 - u_s}{u_0 - u_s}$$

was found from

$$y^2 - [2 + (\frac{u_0 - u_1}{s_0})^2] \, y + 1 = 0$$

to be 0.487. The shock strength was

$$1/y = 2.05,$$

the shock velocity was

$$u_s = u_0 - s_0 y^{-\frac{1}{2}}$$
$$= -17 \text{ km/s},$$

and the shock Mach number was

$$M_s = y^{-\frac{1}{2}} = 1.43.$$

Thus the shock propagated inward very slowly. This is a stable steady state situation, since as the shock moves closer to the critical point its strength (1/y) decreases and it gets dragged back out to where it was.

The Richtmyer type Lagrangian code I used had an artificial viscosity which spread the shock over two zones, and weakened it slightly. The real shock would therefore be stable as well, and would be slightly further in, closer to the inner critical point. The reason for the discrepancy between our results and those of Kopp and Holzer is not known. It may be that their Eulerian code damped their shock more heavily than my artificial viscosity, so that their shock was weaker, and hence got dragged outward by the wind.

These results are presently being written up as a brief research note.

References

Book, D.L.; Boris, J.P. and Hain, K. 1975, J. Comp. Phys. 18, 248.

Hartunian, N. 1975, "Magneto-Acoustic-Gravity Waves", thesis, Brandeis University.

Kato, S. 1966, Astrophys. J. 143, 893.

Klein, R. I., Stein, R.F. and Kalkofen, W. 1977 (submitted to Astrophys. J.)

Kopp, R.A. and Holzer, T.E. 1976, Solar Phys. 49, 43.

Lamb, H. 1945, Hydrodynamics, Dover, N.Y.

MacCormack, R.W. 1971, Proc. 2nd Intl. Conf. on Nun. Meth. in fluid Dyn., Lect. Notes in Phys. Vol. 8, M. Holt ed., Springer-Verlag, N.Y.

Richtmyer, R.D. and Morton, K.W. 1969, "Difference Methods for Initial Value Problems", Interscience Publ., N.Y.

Schmidt, H. and Zirker, J. 1963, Astrophys. J. 138, 1310.

Schwartz, R.A. and Stein, R.F. 1975, Astrophys. J. 200, 499.

Stein, R.F. and Schwartz, R.A. 1972, Astrophys. J. 177, 807.

Vernazza, J.E.; Foukal, P.V.; Huber, M.C.E.; Noyes, R.W.; Reeves, E.M.; Schmahl, E.J.; Timothy, J.G.; and Withbroc, G.L.; 1975, Astrophys. J. Lett. 199, L123.

Figure Captions

Figure 1: Relative intensity fluctuations as a function of time. The relative intensity is shown for six lines formed in the region from the bottom of the transition zone (Ly α) to the low corona (Mg x). Intensity is normalized so maximum intensity is one for each line for each time interval. Temperatures at the right are the approximate formation temperature of the lines.

Figure 2: Velocity as a function of time for an acoustic wave pulse traveling vertically upward through a model solar atmosphere. The velocity amplitude is scaled by $(\text{density})^{1/4}$.

Figure 3: Number of pulses observed in O IV (λ 554) as a function of the time delay between successive pulses. Data from Harvard UV experiment on skylab. Each curve is for pulses greater than indicated strength, as measured by ratio of maximum to base intensity.

Figure 4: Similar to Figure 3, but for C III (λ 977).

Figure 5: Velocity and density amplitude of pulse at bottom ($T=2\times10^{4\circ}K$) and middle ($T=2\times10^{5\circ}K$) of transition region. Note decrease in density but not velocity amplitude of wave in transition region.

Figure 6: Mach number and density vs. height for steady flow through a vertical magnetic flux tube that diverges faster than radially. The flux tube spreads by a factor 4.5 faster than radially at heights near $R_\odot/2$ above the photosphere.

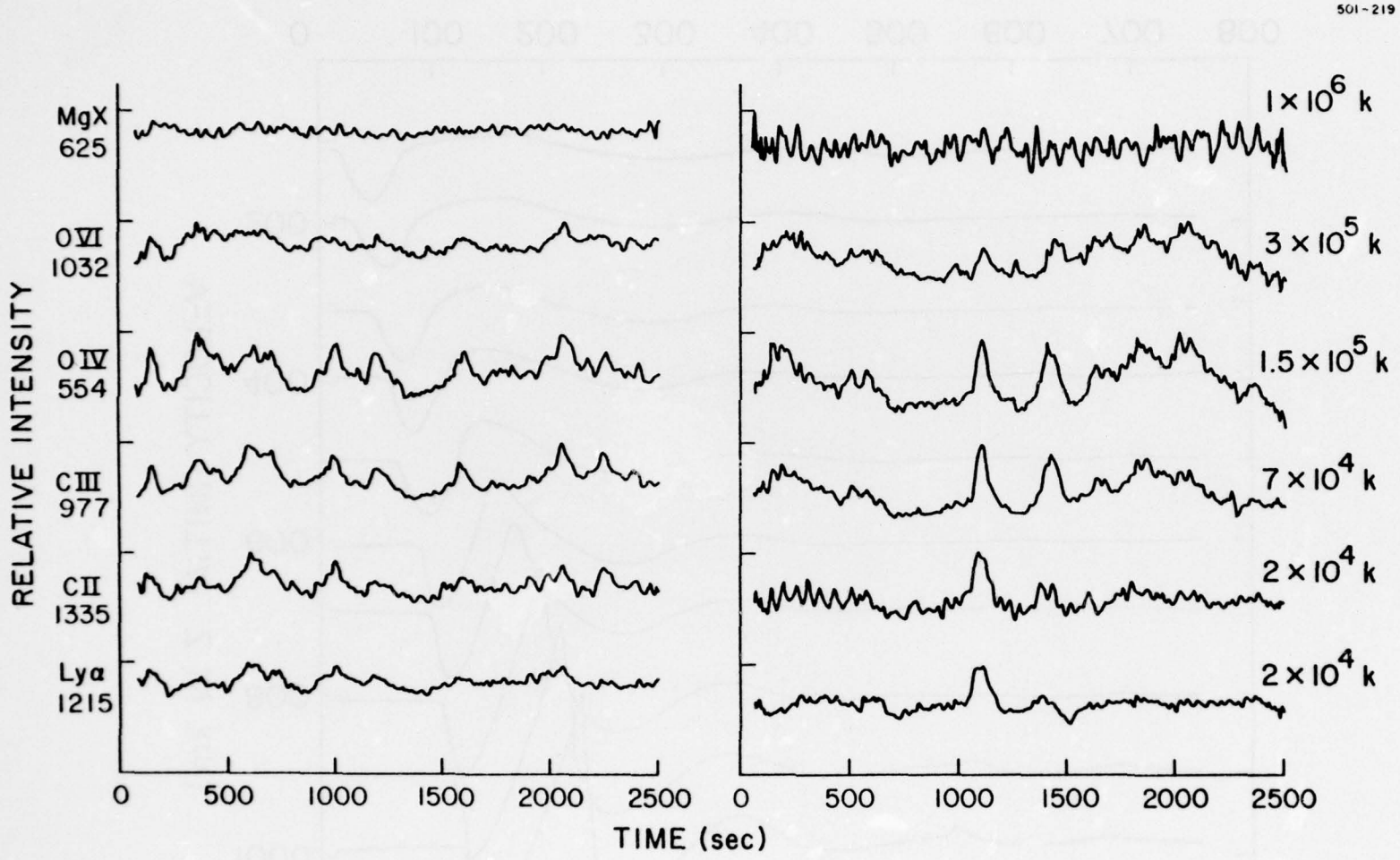
501-219
MgX 625
OVI 1032
OIV 554
CIII 977
CII 1335
Lyα 1215
RELATIVE INTENSITY
1 × 10^6 k
3 × 10^5 k
1.5 × 10^5 k
7 × 10^4 k
2 × 10^4 k
2 × 10^4 k
0
500
1000
1500
2000
2500
TIME (sec)

Figure 1.

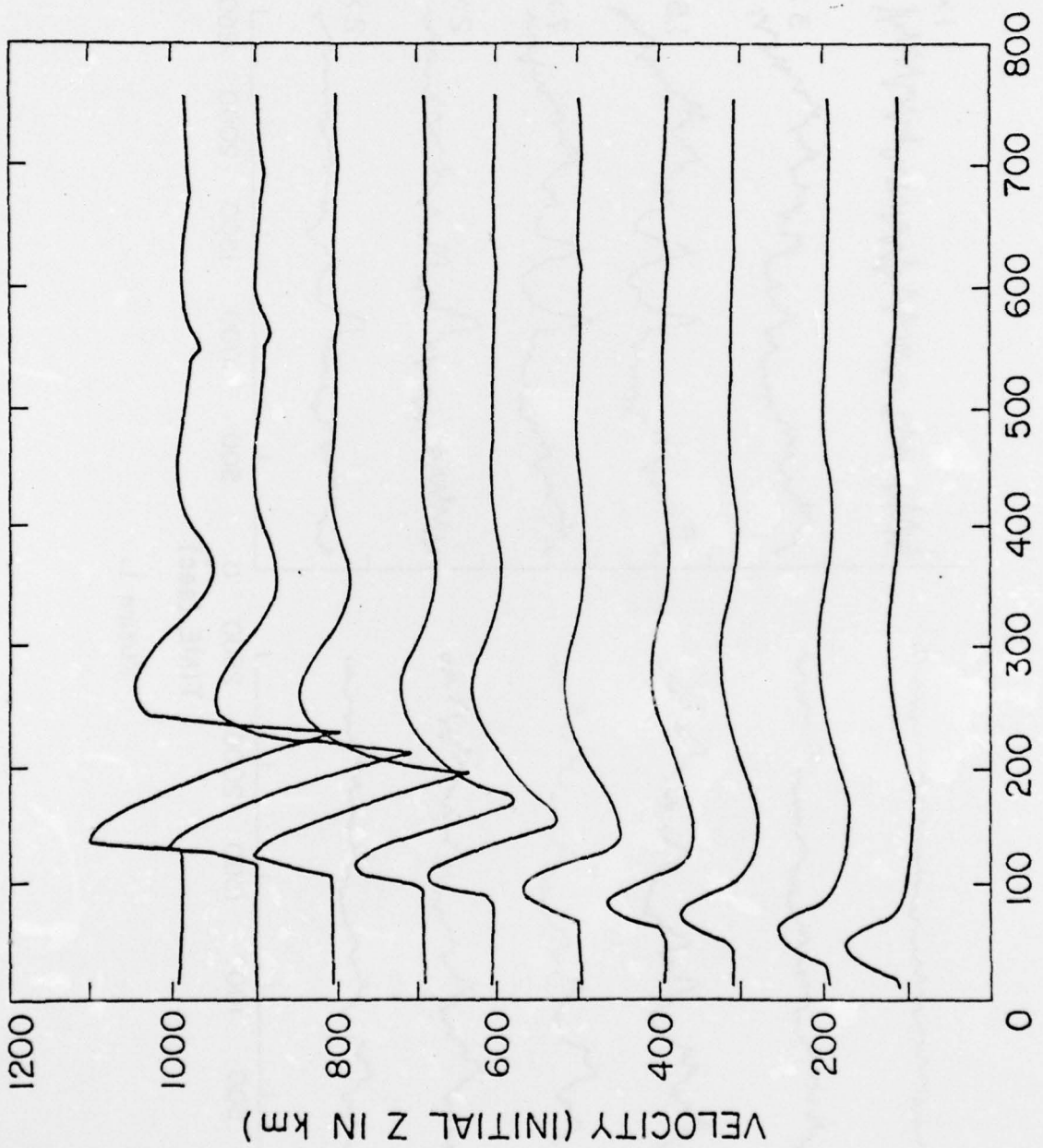
VELOCITY (INITIAL Z IN km)
1200
1000
800
600
400
200
0
100
200
300
400
500
600
700
800
TIME (sec)

Figure 2.

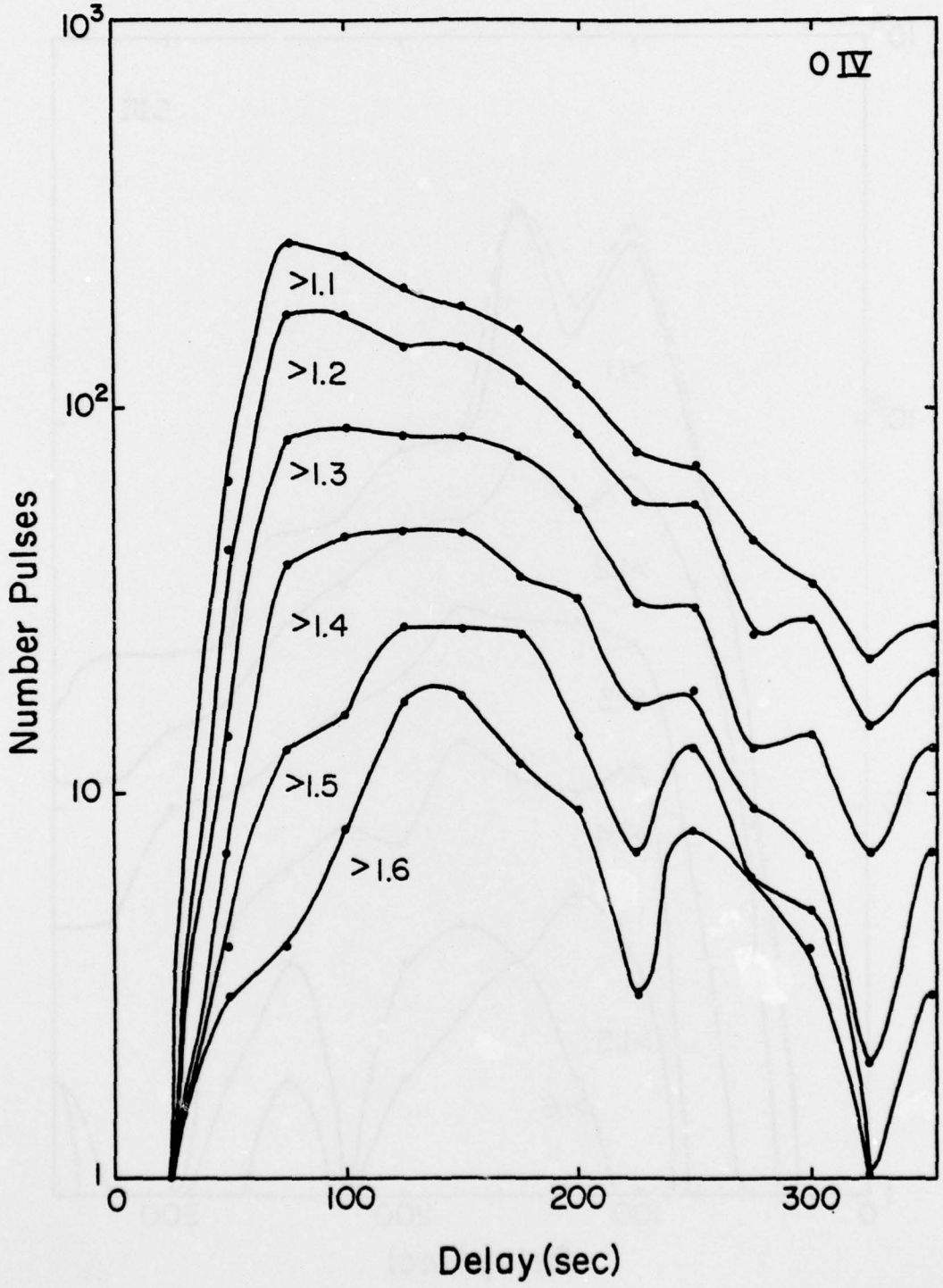
O IV
>1.1
>1.2
>1.3
>1.4
>1.5
>1.6
Number Pulses
Delay (sec)
10³
10²
10
1
0
100
200
300

Figure 3.

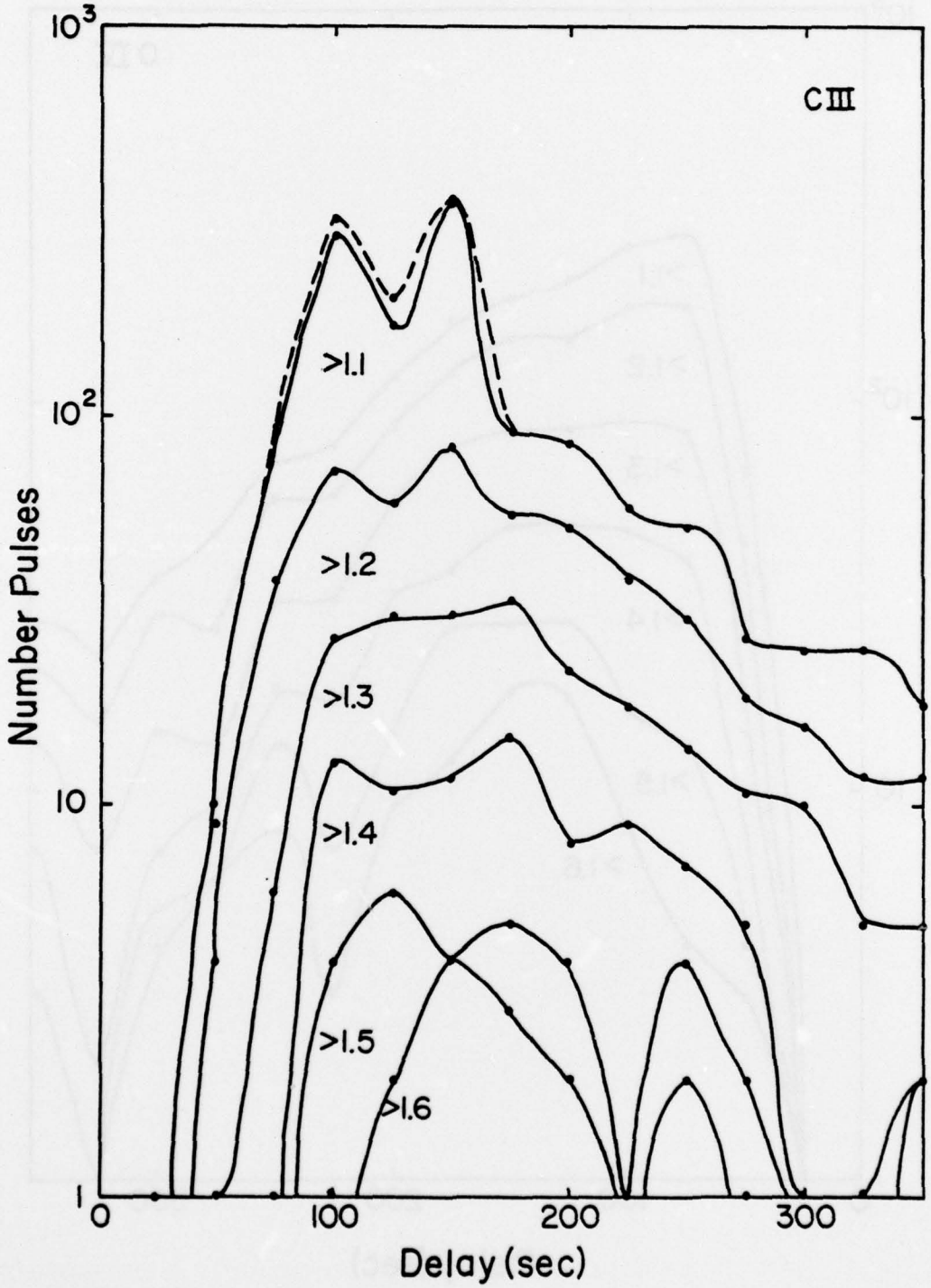
CIII
>1.1
>1.2
>1.3
>1.4
>1.5
>1.6
Number Pulses
Delay (sec)
10³
10²
10
1
0
100
200
300

Figure 4.

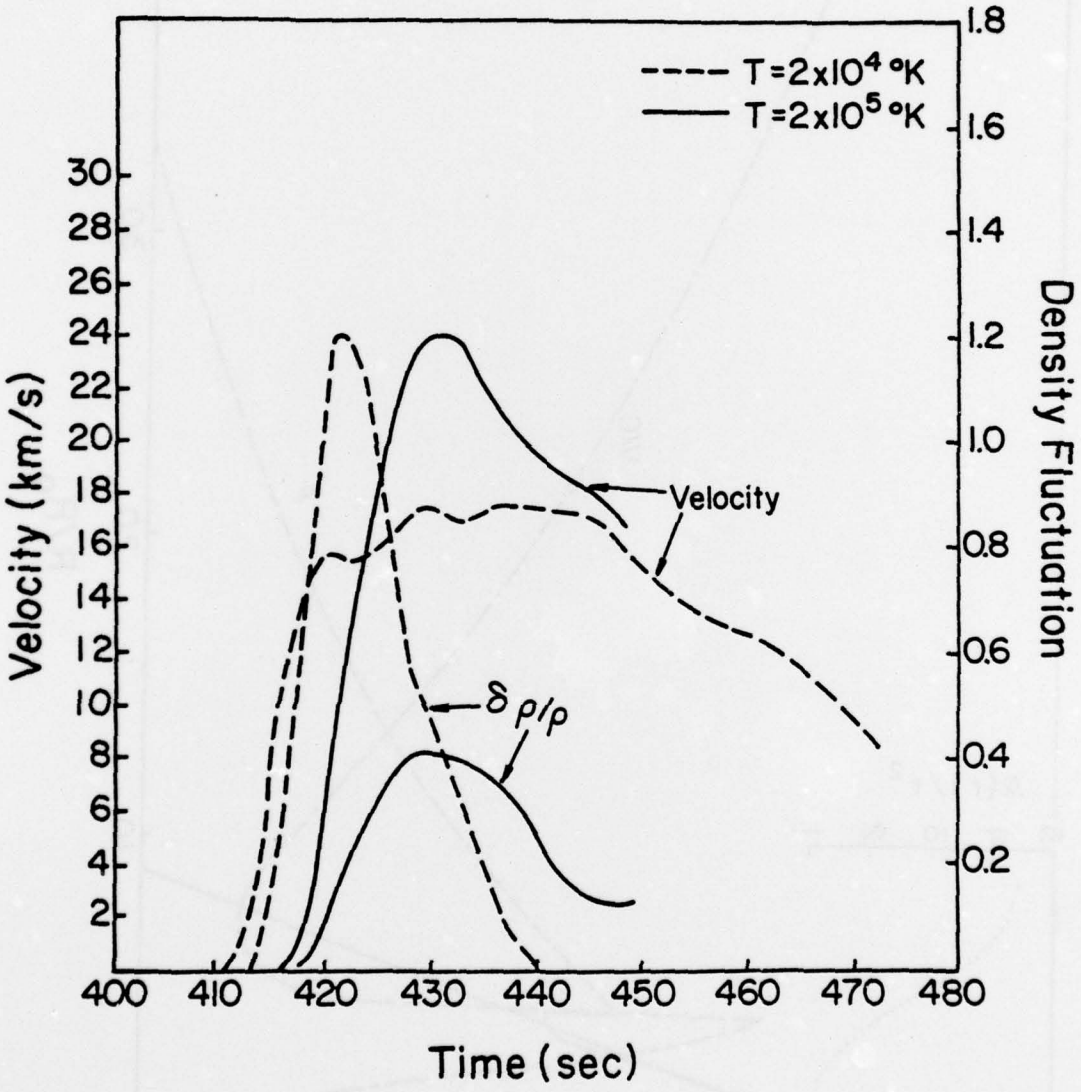
T=2x10⁴ °K
T=2x10⁵ °K
Velocity
δ ρ/ρ
Velocity (km/s)
Density Fluctuation
Time (sec)
30
28
26
24
22
20
18
16
14
12
10
8
6
4
2
1.8
1.6
1.4
1.2
1.0
0.8
0.6
0.4
0.2
400
410
420
430
440
450
460
470
480

Figure 5.

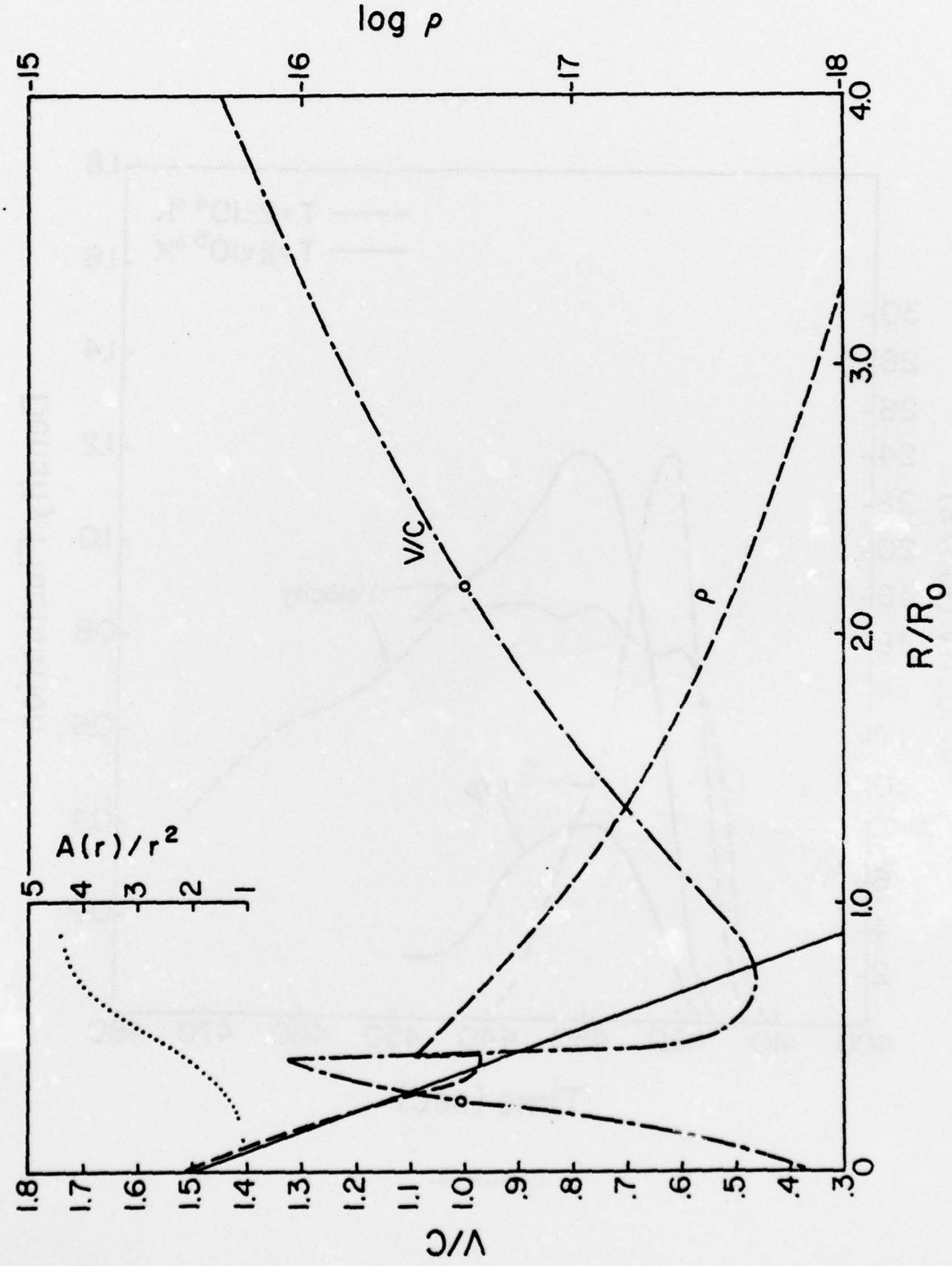
log ρ
-15
-16
-17
-18
4.0
3.0
2.0
1.0
0
R/R₀
V/C
ρ
A(r)/r²
5
4
3
2
1
1.8
1.7
1.6
1.5
1.4
1.3
1.2
1.1
1.0
.9
.8
.7
.6
.5
.4
.3
V/C

Figure 6.